Atmospheric Environment 190 (2018) 269–283

Contents lists available at ScienceDirect

Atmospheric Environment

journal homepage: www.elsevier.com/locate/atmosenv

What drives changes in aerosol properties over the Yangtze River Basin in past four decades ?

Lijie He[a], Lunche Wang[b,c,*], Aiwen Lin[a], Ming Zhang[b], Xiangao Xia[c,d], Minghui Tao[b], Hao Zhou[e]

[a] School of Resource and Environmental Science, Wuhan University, Wuhan, Hubei Province, 430079, China
[b] Laboratory of Critical Zone Evolution, School of Earth Sciences, China University of Geosciences, Wuhan 430074, China
[c] Key Laboratory of Middle Atmosphere and Global Environment Observation (LAGEO), Institute of Atmospheric Physics, Chinese Academy of Sciences, Beijing 100029, China
[d] Collaborative Innovation Center on Forecast and Evaluation of Meteorological Disasters, Nanjing University of Information Science & Technology, Nanjing 210044, China
[e] MOE Key Laboratory of Fundamental Physical Quantities Measurement, School of Physics, Huazhong University of Science and Technology, Wuhan 430074, China

GRAPHICAL ABSTRACT

Trend analysis of monthly mean AOD derived from near–full MERRA–2 (1980-2016), Terra (2000-2016) and Aqua (2002-2016) data records over YRB. The observed AOD values are presented in (a), while the deseasonalized MERRA–2 and MODIS AOD values are respectively shown in (b) and (c).

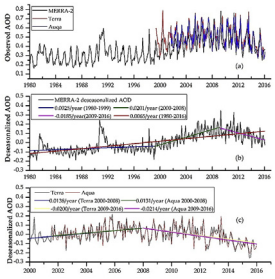

ARTICLE INFO

Keywords:
Aerosol optical depth
Aerosol direct radiative effect
Trend analysis
Impact factor analysis
Yangtze river basin

ABSTRACT

Since the Reform and Opening up in China, aerosols increasingly affect the country's climate change and human health. However, remote sensing studies have been inconclusive as to long-term trends in Chinese aerosol emissions. The newly-released MERRA-2 product provides a long-term (1980 onward) aerosol reanalysis dataset, and thus is used in this study for identifying trends in aerosol optical depth (AOD) and aerosol direct radiative effect (ADRE) in clear sky over the Yangtze River Basin (YRB) based on the MK nonparametric method. Results reveal that there is a notable turning point in AOD trends around 2008, i.e., significantly increasing by 0.0201 $year^{-1}$ before 2008 and then deceasing by -0.0185 $year^{-1}$. The reason may be the decreases of SO_2, NO_x and soot (dust) emissions from major cities in the YRB since 2006. Likewise, the cooling (warming) effects at the top of atmosphere (TOA), surface (SFC) and atmosphere (ATM) strongly increase by -0.3744 and -0.5652 (0.2935) wm^{-2} $year^{-1}$ before 2008, and then significantly decrease by 0.2731 and 0.5868 (-0.3145) wm^{-2} $year^{-1}$. Trend analyses confirm that changes in AOD dominate ADRE trends. Furthermore, AOD is significantly negatively (positively) associated with NDVI and precipitation (GDP and Population density) over most areas of the YRB. Besides, similar spatial trends with AOD are also identified in GDP and NDVI. This indicates that increases in GDP and decreases in NDVI caused by rapid urbanization partly lead to the growth of AOD over the middle and lower reaches of the YRB. However, changes in precipitation and Population density alone may not be the main factors for the increasing AOD.

* Corresponding author. Laboratory of Critical Zone Evolution, School of Earth Sciences, China University of Geosciences, Wuhan 430074, China.
E-mail address: wang@cug.edu.cn (L. Wang).

https://doi.org/10.1016/j.atmosenv.2018.07.034
Received 24 April 2018; Received in revised form 11 July 2018; Accepted 21 July 2018
Available online 26 July 2018

1. Introduction

Aerosols suspended in the atmosphere significantly affect climate changes, directly by scattering and absorbing radiation and indirectly by modifying cloud properties (Charlson et al., 1991; Patadia et al., 2008; Christopher, 2011). Besides, particulate matters with diameters less than 2.5 μm ($PM_{2.5}$) are able to be breathed into the lungs, resulting in various diseases (Guo et al., 2017). Therefore, a series of global and regional studies have been implemented to estimate aerosol direct radiative effect (ADRE) and aerosol optical properties, such as aerosol optical depth (AOD), Ångström exponent (AE) and Single scattering albedo (SSA) by using ground-based Aerosol Robotic Network (AERONET) and China Aerosol Remote Sensing Network (CARSNET) (Che et al., 2009, 2014; Tao et al., 2014; Wang et al., 2015; Kang et al., 2016; Xia et al., 2016; Yu et al., 2016). However, due to sparse distribution and high operating cost of the aerosol ground sites, it is unlikely to provide continuous aerosol measurements (Che et al., 2015). Remote sensing such as Moderate Resolution Imaging Spectroradiometer (MODIS), Multi-angle Imaging Spectroradiometer (MISR), Advanced Very High Resolution Radiometer (AVHRR) and Clouds and the Earth's Radiant Energy System (CERES), is expected as an ideal technology for retrieving aerosols optical and radiative properties (Bilal and Nichol, 2015; Tao et al., 2016; Bilal et al., 2017a; He et al., 2017, 2018; Zhang et al., 2017a, 2017b; Wei et al., 2017). Recently, the newly-released Modern-Era Retrospective Analysis and Research and Application, version 2 (MERRA-2) product has a capacity of providing a long-term (1980 onward) aerosol reanalysis dataset, and thus has been used in present study (Buchard et al., 2015, 2016; 2017; Randles et al., 2017).

Over the past four decades (since the 1978 Reform and Opening up), due to its rapid urbanization and industrialization, China has become one of the major sources of anthropogenic aerosols, causing serious air pollution and climate changes (Guo et al., 2017). However, previous researches have been inconclusive as to long-term trends in Chinese aerosol emissions (Zhang and Reid, 2010; He et al., 2016; Mehta et al., 2016; Alfaro-Contreras et al., 2017; Zhang et al., 2017a, 2018). For example, Zhang and Reid (2010) reported there was a significantly increasing AOD trend in the east coast of China from 2000 to 2009 by using MODIS (Terra) Dark Target aerosol observations. On the contrary, significantly decreasing AOD trends were observed in Beijing (2002-2013) and Xiang He (2005-2012) by using ground-based AOD measurements (Li et al., 2014a). Lately, Zhang et al. (2017a) suggested that there were inconsistent trends in AOD over the East China for the period of 2000–2015 by using Terra, Aqua and MISR data. Likewise, De Leeuw et al. (2017) reported that a significant decrease in MODIS AOD was observed over China during 2006–2009, but there was no significant decrease in ATSR (Along Track Scanning Radiometers) AOD in the same period. These inconsistent satellite-retrieved AOD trends were probably due to the bias in calibration and sampling (Zhang et al., 2017a). Thus, it is necessary to further identify long-term trends in AOD and ADRE both spatially and temporally in China. In this study, the Yangtze River Basin (YRB) in China, a region with various aerosol sources and diverse underlying surfaces, is selected as the region of the interest.

The other objective of this study is to explore what drives the trends in AOD over the YRB. Even though several researches have confirmed that AOD is deeply impacted by precipitation, terrain, NDVI (Normalized Difference Vegetation Index), population and economic development, they don't identify the causes for the changes in AOD (He et al., 2016; Klingmüller et al., 2016; Boiyo et al., 2018). In general, terrain is significantly negatively related with AOD over China (He et al., 2016, 2017). However, as we all known, terrain with no changes is unlikely to be the main factor for aerosol trends. Furthermore, Klingmüller et al. (2016) reported that although AOD was strongly associated with precipitation over the Middle East, changes in precipitation were not consistent with AOD trends, and thereby precipitation alone was unlikely to dominate the increasing AOD trends during 2000–2015. In this study, not only the spatial correlations of AOD with precipitation, NDVI, population density (PD) and GDP are quantified, but also the potential factors which contribute to changes in AOD are identified over the YRB by comparing with their trends.

Generally, this study are performed: (1) to analyze spatial patterns of annual mean AOD and ADRE over the YRB, (2) to identify long-term (1980–2016) trends in AOD and ADRE in clear sky both spatially and temporally, and (3) further explore the potential factors that lead to changes in AOD from 2000 to 2016. Its organization structure is as follows. Section 2 provides satellite-based AOD and ADRE data, natural and socio-economic factor data, and analytical methods. The spatial and temporal distributions of AOD and ADRE trends as well as their correlations with potential factors are presented in Section 3. Finally, Section 4 provides a conclusion.

2. Data and methods

2.1. Data

2.1.1. AOD data

The MODIS instrument aboard the Terra (2000 onward) and Aqua (2002 onward) provides aerosol standard products in 36 wavelengths ranging from 0.4 μm to 14.4 μm (https://ladsweb.modaps.eosdis.nasa.gov/). Generally, there are Dark Target (DT) and Deep Blue (DB) algorithm to retrieve AOD values, respectively over vegetated and bright land surfaces (Sayer et al., 2014; Bilal et al., 2017b, 2018). Recently, the MODIS Collection 6 (C6) provide a set of DT and DB merged AOD data (DTB), which has broader spatial coverage and higher accuracy than any single DB and DT algorithm (He et al., 2018). In this study, the monthly high-quality DTB aerosol products are used for estimating AOD at 550 nm trend over the YRB (Table 1). The study period is respectively from March 2000 to December 2016 (Terra) and from July 2002 to December 2016 (Aqua). Note that AOD at 550 nm is abbreviated as AOD in this study.

The MERRA-2 is an atmosphere reanalysis dataset from the NASA Global Modeling and Assimilation Office (GMAO). By assimilating bias-corrected AOD data from MODIS, AVHRR, MISR (over bright surface) and AERONET (Level 2.0), the MERRA-2 provides AOD reanalysis datasets (1980 onward) with a spatial resolution of 0.5° × 0.625° (latitude × longitude) through http://disc.sci.gsfc.nasa.gov/mdisc/. More details about the assimilating algorithm of the MERRA-2 AOD

Table 1
Statistics of MODIS (Terra and Aqua), MERRA-2 and CARSNET AOD data used in this study for the period of 1980–2016 over the YRB.

Application	Sensor	Product	Spatial resolution (Latitude × Longitude)	Temporal resolution/coverage	Quality flag
AOD trend analysis	Terra	MOD08	1° × 1°	monthly/2000–2016	3.0
	Aqua	MYD08	1° × 1°	monthly/2002–2016	3.0
	MERRA-2	insM_2d_gas_Nx	0.5° × 0.625°	monthly/1980–2006	cloud-screened
AOD validation	MERRA-2	ins3_2d_gas_Nx	0.5° × 0.625°	daily /2007–2012	cloud-screened
	CARSNET	\	\	daily /2007–2012	2.0

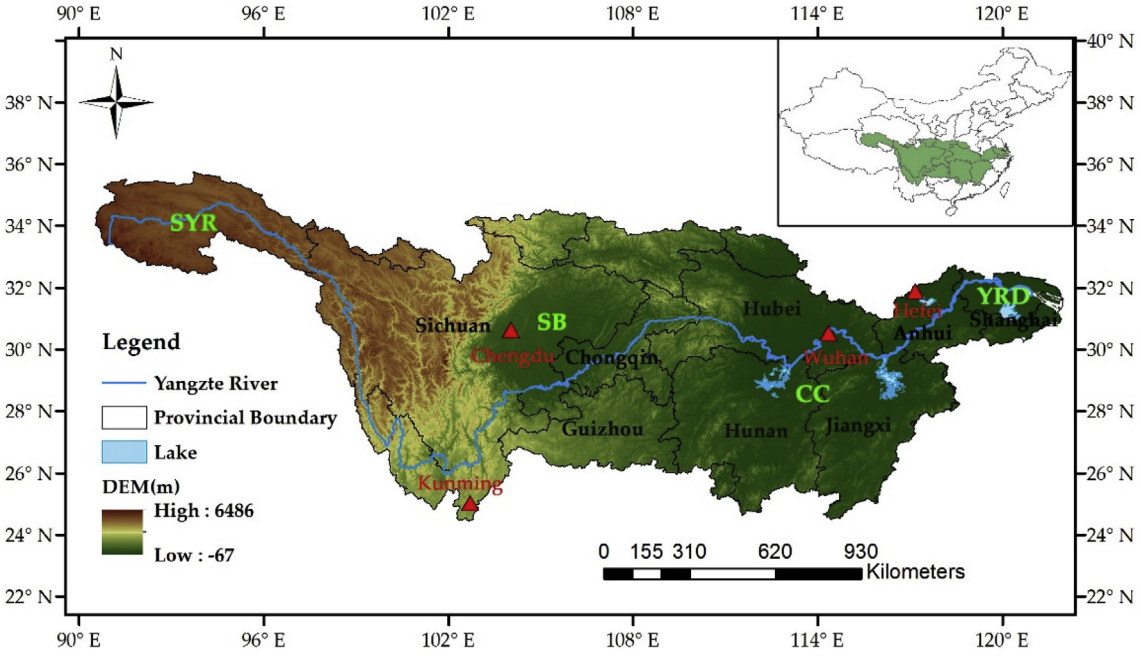

Fig. 1. Elevation map of the Yangtze River Basin (YRB). The red triangles refer to the China Aerosol Remote Sensing Network (CARSNET) ground-based aerosol sites, from east to west, followed by Hefei, Wuhan, Sichuan and Kunming. The YRD, CC, SB and SYR are the Yangtze River Delta, Central China, Sichuan Basin and the Source of the Yangtze River, respectively. (For interpretation of the references to colour in this figure legend, the reader is referred to the Web version of this article.)

reanalysis data have been described in previous researches (Buchard et al., 2015, 2016; 2017; Randles et al., 2017). In this study, the monthly MERRA-2 AOD reanalysis datasets are used for identifying AOD trends during January 1980–December 2016 over YRB (Table 1).

Furthermore, in order to evaluate the performance of the MERRA-2 AOD reanalysis data, the daily ground-based AOD observations are obtained from four CARSNET ground sites over the YRB from 2007 to 2012 (Fig. 1). Similar to the AERONET, the CARSNET is also a common ground-based aerosol network around China, which retrieves aerosol observations at four wavelengths ranging from 340 nm to 1020 nm by using the CIMEL sun photometer. Due to no AOD values at 550 nm, the daily CARSNET AOD at 550 nm (Level 2.0, quality assured) observations need to be calculated by Equations (1) and (2).

$$AOD_{\lambda_i} = \beta\lambda_i^{-\alpha} \tag{1}$$

$$\alpha = \frac{\ln(AOD_{\lambda_1}/AOD_{\lambda_2})}{\ln(\lambda_1/\lambda_2)}, \quad \beta = \frac{AOD_{\lambda_1}}{\lambda_2^{-\alpha}} \tag{2}$$

Where α is the Ångström exponent, β is the turbidity coefficient, λ_1 and λ_2 refer to the 440 nm and 870 nm wavelengths, respectively. The validation results are shown in Fig. 2. There are 1814 CARSNET-MERRA-2 AOD matchups, with a high correlation coefficient (R = 0.90) at 95% significant level ($p < 0.05$). It demonstrates that the MERRA-2 AOD reanalysis datasets agree well with the CARSNET AOD observations over the YRB. Similar high correlation coefficients (> 0.8) were also found at nearly 40 ground-based aerosol sites over the global land (Randles et al., 2017). In a word, both the previous and the current validation results provide high confidence in using MERRA-2 AOD reanalysis data for aerosol applications over the YRB.

2.1.2. ADRE data

In clear sky, ADRE is defined as the difference in the net (downward ↓ minus upward ↑) shortwave radiation flux with and without aerosols at TOA (Equation (3)), SFC (Equation (4)) and ATM (Equation (5)).

$$ADRE_{TOA} = (F_{aero}\downarrow - F_{aero}\uparrow)_{TOA} - (F_{clr}\downarrow - F_{clr}\uparrow)_{TOA} \tag{3}$$

$$ADRE_{SFC} = (F_{aero}\downarrow - F_{aero}\uparrow)_{SFC} - (F_{clr}\downarrow - F_{clr}\uparrow)_{SFC} \tag{4}$$

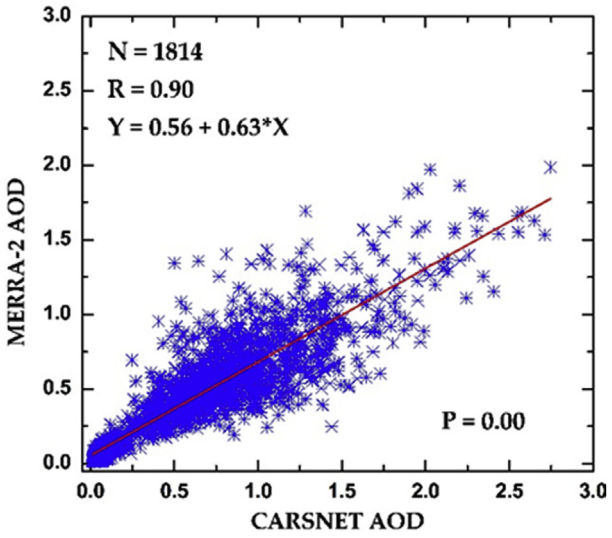

Fig. 2. The comparison of the daily CARSNET AOD observations and the corresponding MERRA-2 AOD during 2007–2012 over YRB.

$$ADRE_{ATM} = ADRE_{TOA} - ADRE_{SFC} \tag{5}$$

where $(F_{aero}\downarrow - F_{aero}\uparrow)$ and $(F_{clr}\downarrow - F_{clr}\uparrow)$ refer to the net shortwave radiation flux with and without aerosols, respectively. If ADRE > 0, aerosols exert a warming effect at the TOA, SFC and ATM; otherwise there is a cooling effect. In this study, the monthly ADRE grid data (0.5° × 0.625°) are calculated from the MERRA-2 radiative fluxes reanalysis dataset (tavgM_2d_rad_Nx) for the period of January 1980–December 2016 over YRB. More detailed descriptions about the tavgM_2d_rad_Nx reanalysis dataset see Table 2.

2.1.3. Natural and socio-economic data

In order to explore which natural and socio-economic factors drive AOD trends, the Normalized Difference Vegetation Index (NDVI), precipitation, Gross Domestic Product (GDP) and Population Density (PD)

Table 2
Description of the MERRA-2 radiation flux reanalysis dataset (tavgM_2d_rad_Nx) used in this study.

Scientific Data set (SDS)	Description	Corresponding Parameter
SWTNTCLR	toa_net_downward_shortwave_flux_in_clear_sky	$(Faero\downarrow - Faero\uparrow)_{TOA}$
SWTNTCLRCLN	toa_net_downward_shortwave_flux_in_clear_sky_and_no_aerosol	$(Fclr\downarrow - Fclr\uparrow)_{TOA}$
SWGNTCLR	surface_net_downward_shortwave_flux_in_clear_sky	$(Faero\downarrow - Faero\uparrow)_{SFC}$
SWGNTCLRCLN	surface_net_downward_shortwave_flux_in_clear_sky_and_no_aerosol	$(Fclr\downarrow - Fclr\uparrow)_{SFC}$

data are collected for the period of January 2000–December 2016 over the YRB. These data sources are as follows: (1) the monthly MODIS C6 Level3 NDVI product (MCD13) with a spatial resolution of 0.05° (https://ladsweb.modaps.eosdis.nasa.gov/), (2) the monthly TRMM3B42 (Tropical Rainfall Measuring Mission) precipitation data with a spatial resolution of 0.25° (http://www.gscloud.cn/), and (3) the yearly GDP and PD grid data (1 km) provided by Data Center for Resources and Environmental Sciences, Chinese Academy of Sciences (RESDC) (http://www.resdc.cn).

2.2. Methods

2.2.1. Trend analysis method

Long-term (1980 onward) annual trends in AOD and ADRE over the YRB are estimated as follows. Firstly, in order to get rid of the seasonal interference, the AOD and ADRE datasets are preprocessed by the harmonic regression (Young et al., 1999). Then, a linear regression analysis is adopted to quantify annual trends in AOD and ADRE for the period of 1980–2016 over the YRB. It can be expressed as (Equation (6)):

$$Y_t = C + \omega * X_t + \varepsilon \tag{6}$$

where Y_t refers to the AOD and ADRE values, X_t represents time, C is the offset which means the AOD and ADRE values at the beginning time, ε is the error term, and ω is the slope, i.e., the trend. Finally, AOD and ADRE trends are further tested for their statistics significance by using the MK nonparametric method. The statistics S is defined as:

$$S = \sum_{i=1}^{n-1} \sum_{j=n+1}^{n} sgn(X_j - X_i) \tag{7}$$

where X_j and X_i are the AOD and ADRE values corresponding to the year j and i in the time series, n is the length of the time series, $sgn(X_j - X_i)$ is the sign function expressed as:

$$sgn(X_j - X_i) = \begin{cases} +1, & if\ (X_j - X_i) > 0 \\ 0, & if\ (X_j - X_i) = 0 \\ -1, & if\ (X_j - X_i) < 0 \end{cases} \tag{8}$$

If S is approximately normal distribution, then the variance becomes:

$$Var(s) = \frac{n(n-1)(2n+5) - \sum_{i=1}^{p} t_i(t_i-1)(2t_i+5)}{18} \tag{9}$$

where t_i is the tied value corresponding to the ith number. And the standard normal test statistics Z used for identifying a significant trend is calculated by:

$$Z = \begin{cases} \frac{S-1}{\sqrt{Var(S)}}, & if\ S > 0 \\ 0, & if\ S = 0 \\ \frac{S+1}{\sqrt{Var(S)}}, & if\ S < 0 \end{cases} \tag{10}$$

If Z > 0, the trend increases with time, otherwise it decreases. However, only when $|Z| > |Z_{(1-\alpha/2)}|$, the null hypothesis is rejected, indicating that there is a significant trend. When the significant level α = 1%, 5%, and 10%, their corresponding $|Z_{(1-\alpha/2)}|$ are respectively 2.58, 1.96 and 1.65.

2.2.2. Correlation analysis method

Linear regression is adopted to analyze the correlation between AOD and its potential natural and socio-economic impact factors including NDVI, Precipitation, GDP and PD data. The higher the correlation coefficient (R) is, the stronger the relationships become. In addition, the statistics significance in the R is further examined by the T-test method, which is expressed as:

$$t = R\sqrt{\frac{(n-2)}{(1-R^2)}} \tag{11}$$

here n is the number of the observations. Generally, correlation is considered as significant at a 95% confidence level, i.e., $p < 0.05$. However, due to the different spatial resolutions of these datasets used in the correlation analysis, we need to first preprocess AOD and its impact factor data by reprojection, mosaicking and resampling. In this way, the per-pixel (1° × 1°) R value and its corresponding p value are calculated from monthly NDVI and Precipitation as well as yearly GDP and PD observations for the period of January 2000–December 2016.

3. Results and discussion

3.1. Spatial distribution of annual mean AOD and ADRE

The spatial distribution of 37-year average (from 1980 to 2016) MERRA-2 AOD and ADRE over the YRB is presented in Fig. 3. Clearly in Fig. 3(a), high AOD values (> 0.5) are observed over the regions with strong anthropogenic activities, such as the Sichuan Basin (SB), Central China (CC) and Yangtze River Delta (YRD).However, there are low aerosol loadings (< 0.3) in the mountains over the Source of Yangtze River (SYR). Similar AOD spatial patterns over the YRB were reported in previous studies (He et al., 2017, 2018). As shown in Fig. 3(b) and (c), the $ADRE_{TOA}$ and $ADRE_{SFC}$ values in clear sky are all negative, indicating that aerosols exert cooling effects at the TOA and SFC. However, there is a warming effect for aerosols in the atmosphere due to the positive $ADRE_{ATM}$ values in Fig. 3(d). In terms of the spatial distribution of ADRE in clear sky, strong cooling effects at the TOA ($ADRE_{TOA} < -10\ wm^{-2}$) and SFC ($ADRE_{SFC} < -20\ wm^{-2}$) are observed over the SB, CC and YRD, while there are weak cooling effects for $ADRE_{TOA}$ (> -4 wm^{-2}) and $ADRE_{SFC}$ (> -10 wm^{-2}) over the SYR. Similar spatial patterns of $ADRE_{ATM}$ in clear sky are illustrated in Fig. 3(d), but the difference is that there is a warming effect for aerosols at the ATM. Nevertheless, it is easy to find that ADRE at the TOA, SFC and ATM are all closely related with AOD in spatially.

In order to clarify their relationship, the correlation coefficient (R) is quantified by using 37-year monthly MERRA-2 AOD and ADRE reanalysis data, and the corresponding calculation result is shown in Fig. 4. Pixels with significant correlation ($p < 0.05$) are marked with a dot. In Fig. 4(a) and (b), the significant negative correlation ($R < -0.8$) of AOD with $ADRE_{TOA}$ and $ADRE_{SFC}$ is identified over broad areas of the YRB. That is to say, the larger the AOD values are, the lower the negative $ADRE_{TOA}$ and $ADRE_{SFC}$ values are, and thus the stronger the cooling effects for aerosols at the TOA and SFC become. Notably, there is a relative low |R| for both AOD-$ADRE_{TOA}$ and AOD-$ADRE_{SFC}$ over the Sichuan Basin. This may be attributed to its unique basin terrain (Tao et al., 2014). On the contrary, AOD is significantly positively correlated with $ADRE_{ATM}$ ($R > 0.8$) over the middle and

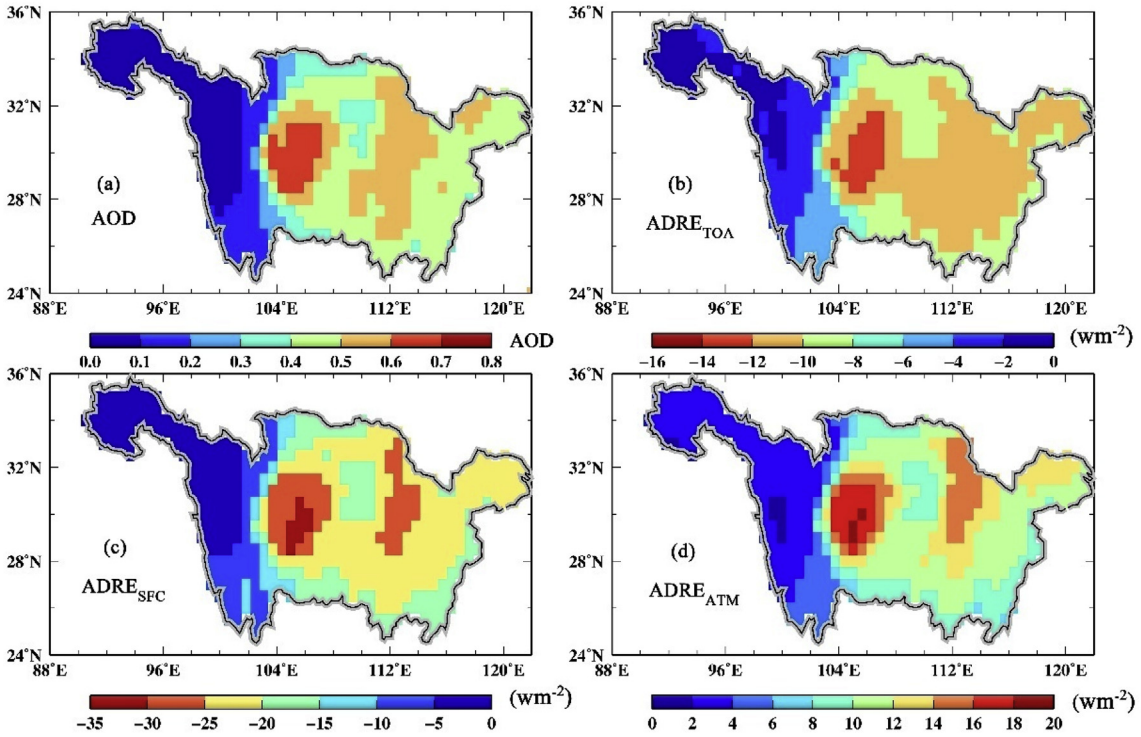

Fig. 3. Spatial distribution of the annual mean AOD (a), ADRE$_{TOA}$ (b), ADRE$_{SFC}$ (c) and ADRE$_{ATM}$ (d) derived from the monthly MERRA-2 aerosol reanalysis dataset for the period of 1980–2016 over YRB.

lower reaches of the YRB. Meanwhile, the positive correlation of AOD-ADRE$_{ATM}$ gradually increases from the Northwest to the Southeast. High correlation between AOD and ADRE was also reported over the Beijing (Yu et al., 2016), YRD (Kang et al., 2016), China (Xia et al., 2016), Southeast Asia (Feng and Christopher, 2014) and global ocean (Alfaro-Contreras et al., 2017).

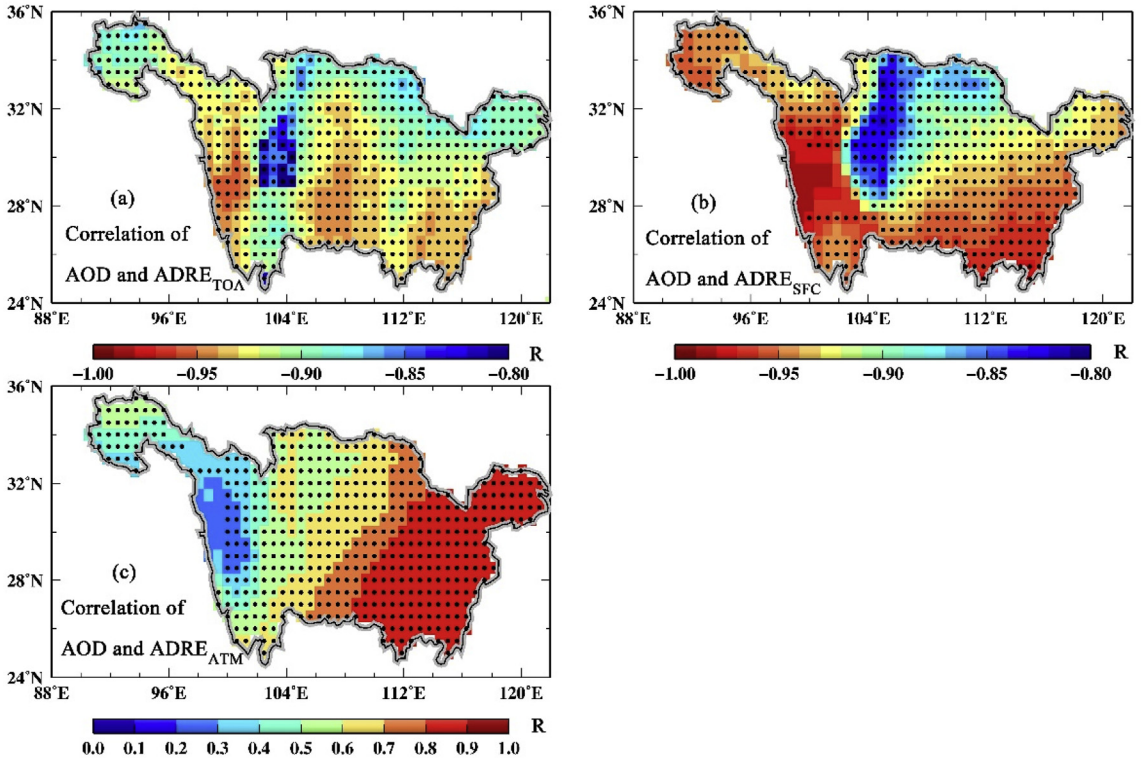

Fig. 4. Correlation coefficient (R) of monthly mean ADRE$_{TOA}$ (a), ADRE$_{SFC}$ (b) and ADRE$_{ATM}$ (c) with AOD derived from the MERRA-2 aerosol reanalysis dataset for the period of 1980–2016 over YRB. Pixels with significant correlation ($p < 0.05$) are marked with a black dot.

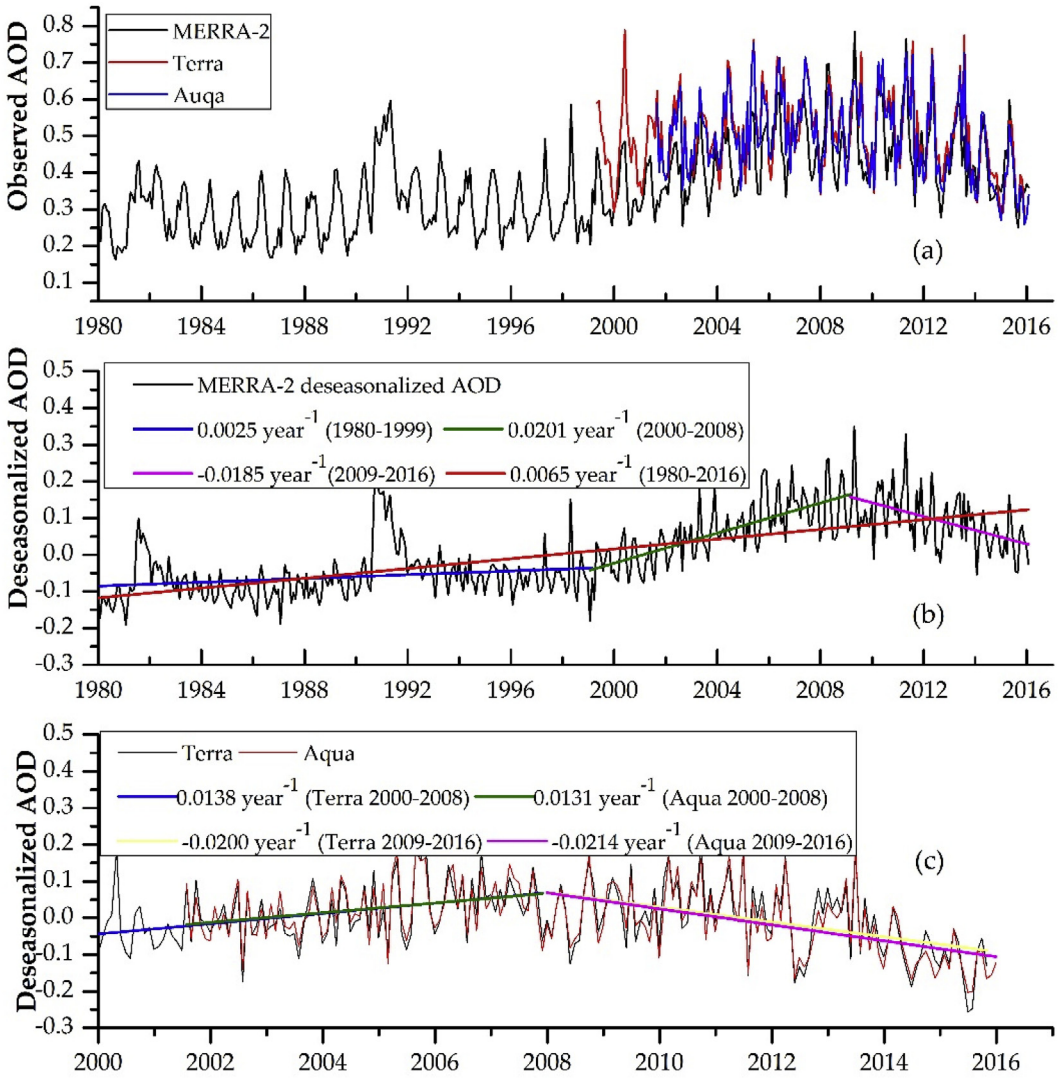

Fig. 5. Trend analysis of monthly mean AOD derived from near–full MERRA–2 (1980-2016), Terra (2000-2016) and Aqua (2002-2016) data records over YRB. The observed AOD values are presented in (a), while the deseasonalized MERRA–2 and MODIS AOD values are respectively shown in (b) and (c).

3.2. Trend analysis of AOD and ADRE

3.2.1. AOD trend

Fig. 5(a) shows the monthly variation of AOD observations derived from the near-full (1980-2016), Terra (2000-2016) and Aqua (2002-2016) data records over the YRB. The correlation coefficient values of the monthly mean MERRA-2 AOD with Terra and Aqua AOD are 0.65 and 0.72, respectively. This indicates that the MERRA-2 aerosol re-analysis dataset agrees well with the MODIS AOD retrievals over the YRB. Then, their deseasonalized AOD values by using the harmonic regression are shown in Fig. 5(b) (MERRA-2) and Fig. 5(c) (Terra and Aqua). Overall, for the entire study period (1980–2016), there is a slight upward trend (0.0065 $year^{-1}$) at 95% significant level ($p = 0.00$) for MERRA-2 deseasonalized AOD. Before 2000, the increase in AOD is not obvious with a trend of 0.0025 $year^{-1}$. Notably, there is a severe growth for aerosol loading in 1982 and 1991, probably due to the eruption of the El Chichon in Mexico and the Pinatubo in the Philippines, respectively (McCormick and Swissler, 1983; Dutton and Christy, 1992). However, the period of 2008–2009 appears to be a pivot point in AOD trends. During 2000–2008, strong continuous upward AOD trends are observed for all three sensors, but the growth magnitude for MERRA-2 (0.0201 $year^{-1}$) is larger than those of Terra (0.0138 $year^{-1}$) and Aqua (0.0131 $year^{-1}$). Likely, the slight difference in AOD trends between MERRA-2 and MODIS is caused by bias in sampling and calibration (Zhang et al., 2017a; Alfaro-Contreras et al., 2017). The increase in AOD during 2000–2008 may be in response to rapid urbanization and economic growth (De Leeuw et al., 2017). However, during 2009–2016, there is a significant downward trend for MERRA-2 (-0.0185 $year^{-1}$), Terra (-0.0200 $year^{-1}$) and Aqua (-0.0214 $year^{-1}$). The decrease in AOD since 2008, may be associated with the 2008 Beijing Olympic Games when the air pollution in China has been highlighted in media, and thus a series of emission reduction measures have been implemented. Also, it may be partly caused by the 2008 global economic crisis (He et al., 2016). As illustrated in Fig. 6, since 2006, the total emissions of SO_2 and soot (dust) from major provinces over the YRB, begin to decline continuously. And also NO_x emissions reduce from 2011 to 2015. Despite of a lag effect, AOD trends are consistent with those of pollution emissions. This confirms that decreases of SO_2, NO_x and soot (dust) emissions are the main factor for the downward trend in AOD since 2008. Recently, as shown in Table 3, a turning point around 2008 in AOD trend was also identified by several authors in mainland China (He et al., 2016; Alfaro-Contreras et al., 2017; De Leeuw et al., 2017) and the East Coast of China (Zhang et al.,2017a) by using MODIS and MISR aerosol datasets.

In order to identify the spatial parttern in AOD trend from MERRA-2, Terra and Aqua over YRB, we have performed AOD saptial trend

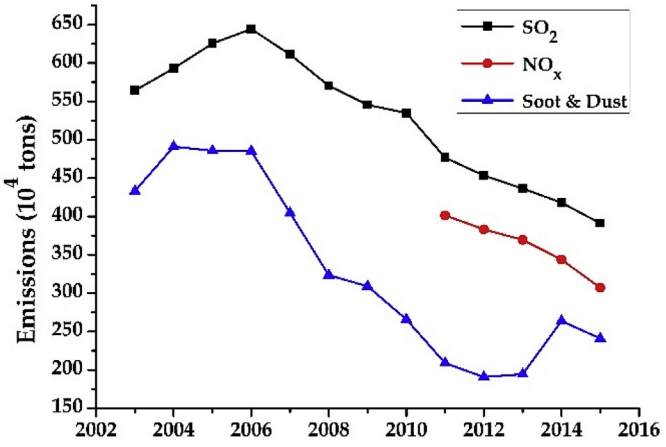

Fig. 6. Total emissions of SO_2, NO_x and soot (dust) from major provinces over the YRB, including Shanghai, Jiangxi, Hubei, Hunan, Chongqing, Sichuan and Guizhou. The data is provided by China National Bureau of Statistics (http://www.stats.gov.cn/).

analysis by using a linear regression and detected its corresponding significant level based on the MK method. The trend analysis results are shown in Fig. 7, where the pixels at 95% significant level ($p < 0.05$) are marked with a dots. As illustrated in Fig. 7, the significant AOD trends always prevail over the SB and the middle and lower reaches of YRB. Generally, over the most areas of the YRB, the spatial distribution in AOD trend is similar to its temporal trend. During 2000–2008 (Fig. 7 (a)), strong upward MERRA-2 AOD trends (> 0.025 year^{-1}) are observed over the SB, CC and YRD, where frequent industrialization and urbanization take place. However, there are no significant trends (< 0.010 year^{-1}) over the SYR. Similar spatial patterns in AOD trends during 2000–2008 are also presented in Terra (Fig. 7 (e)) and Aqua (Fig. 7 (g)). Nevertheless, several differences take place. On the one hand, the magnitude of the significant upward AOD trend in Terra and Aqua is lower than that in MERRA-2. On the other hand, a few significant downward AOD trends in Terra and Aqua are observed over the SYR for 2000–2008. Furthermore, during 2009–2016, there is a strong downward AOD trend ($<$ -0.020 year^{-1}) over the SB, CC and YRD, derived from all the MERRA-2 (Fig. 7 (d)), Terra (Fig. 7 (f)) and Aqua (Fig. 7 (h)). Notably, several significant upward AOD trends in Terra and Aqua are found over the less-developed SYR. If AOD trend continues to rise, it will be an alarm for the air quality in these regions.

3.2.2. ADRE trend

Fig. 8 shows the monthly variation of MERRA-2 ADRE observations (black line) at the TOA (Fig. 8(a)), SFC (Fig. 8(b)) and ATM (Fig. 8(c)) in clear sky for the period of 1980–2016 over the YRB. Generally from 1980 to 2016, $ADRE_{TOA}$ ($ADRE_{SFC}$) observations are all negative with the multi-year monthly average of -7.38 Wm^{-2} (-16.73 Wm^{-2}). However, there is a warming effect for aerosols in the atmosphere, due to the positive $ADRE_{ATM}$ values with its multi-year monthly average of 9.89 Wm^{-2}. By using different radiation transfer models and satellite datasets, similar multi-year monthly mean ADRE values at the TOA in clear sky were simulated over the East Asia ($-6.77 \sim -3.43$ Wm^{-2}) and East China (-5.1 Wm^{-2}) (Huang et al., 2007, Sundstrom et al., 2014). And also, Zhuang et al. (2014) reported that annual mean $ADRE_{TOA}$ and $ADRE_{SFC}$ were respectively about -6.9 Wm^{-2} and -21.3 Wm^{-2} over Nanjing city of the YRD from 2011 to 2012.

Fig. 8 also estimates ADRE trends at the TOA, SFC and ATM by using MERRA-2 deseasonalized ADRE datasets (blue line) from 1980 to 2016. All the ADRE trends are detected at 95% significant level, except the trend in $ADRE_{TOA}$ during 1980–1999 ($p = 0.3972$). Clearly, there are opposite trend variations for $ADRE_{TOA}$ (Fig. 8(a)) and $ADRE_{SFC}$ (Fig. 8(b)) with the MERRA-2 AOD (Fig. 5(b)). The reason is that the ADRE over YRB is deeply impacted by AOD, as illustrated in Fig. 4. The detailed $ADRE_{TOA}$ and $ADRE_{SFC}$ trends are elaborated as follows. Before 2000, there are negligible downward trends in $ADRE_{TOA}$ (-0.0216 Wm^{-2} year^{-1}) and $ADRE_{SFC}$ (-0.1317 Wm^{-2} year^{-1}), indicating that the cooling effects for aerosols at the AOT and SFC are slightly increased. And then strong downward trends are observed in $ADRE_{TOA}$ (-0.3744 Wm^{-2} year^{-1}) and $ADRE_{SFC}$ (-0.5652 Wm^{-2} year^{-1}) from 2000 to 2008. On the contrary, there are significant upward trend in $ADRE_{TOA}$ (0.2731 Wm^{-2} year^{-1}) and $ADRE_{SFC}$ (0.5868 Wm^{-2} year^{-1}) from 2009 to 2016, an indication that the cooling effects for aerosols at the AOT and SFC are obviously decreased. Nevertheless, for the whole study period of 1980–2016, the cooling effects at the TOA and SFC experience a slight increase, due to the downward trends in $ADRE_{TOA}$ (-0.0822 Wm^{-2} year^{-1}) and $ADRE_{SFC}$ (-0.2342 Wm^{-2} year^{-1}). In terms of the $ADRE_{ATM}$ trend, it is consistent with the AOD trend: slight upward trend (0.1343 Wm^{-2} year^{-1}) for 1980-1999, strong upward trend (0.2935 Wm^{-2} year^{-1}) for 2000-2008 and significant downward trend (-0.3145 Wm^{-2} year^{-1}) for 2009-

Table 3
Comparisons with previous studies on the trends of AOD and ADRE in China.

Reference	Study Area	Data	AOD trends	ADRE trends
He et al. (2016)	Mainland China	MYD04	↑+0.0003 month^{-1} pre-2008 ↓-0.0005 month^{-1} post-2008	\
Mehta et al. (2016)	China	MODIS MISR	↓decrease (2001-2014)	\
Alfaro-Contreras et al. (2017)	China Coast	MOD04	↑+0.069 decade^{-1}(2000-2015)	\
		MYD04	↓-0.035 decade^{-1} (2002-2015)	\
		MISR	↓-0.014 decade^{-1} (2000-2015)	\
De Leeuw et al. (2017)	Mainland China	ATSR MOD08	↑increase before 2000 ↓decrease after 2011	\
Zhang et al. (2017a)	China North Coast	MOD04	↑~+0.1 (2000-2007) ↓~-0.008 (2008-2015)	\
	China South Coast	MYD04	↑increase (2000-2007) ↓~-7% (2008-2015)	\
This Study	YRB of China (24–36°N 88–123°E)	MERRA-2	↑+0.0065 year^{-1} (1980-2016) ↑+0.0201 year^{-1} (2000-2008) ↓-0.0185 year^{-1} (2009-2016)	↓-0.0822 year^{-1} TOA (1980-2016) ↓-0.2342 year^{-1} SFC (1980-2016) ↑+0.152 year^{-1} ATM (1980-2016)
		Terra MODIS	↑+0.0138 year^{-1} (2000-2008) ↓-0.0200 year^{-1} (2009-2016)	\
		Aqua MODIS	↑+0.0131 year^{-1} (2000-2008) ↓-0.0214 year^{-1} (2009-2016)	\

↑ and ↓ represent the increasing and decreasing trend, respectively.

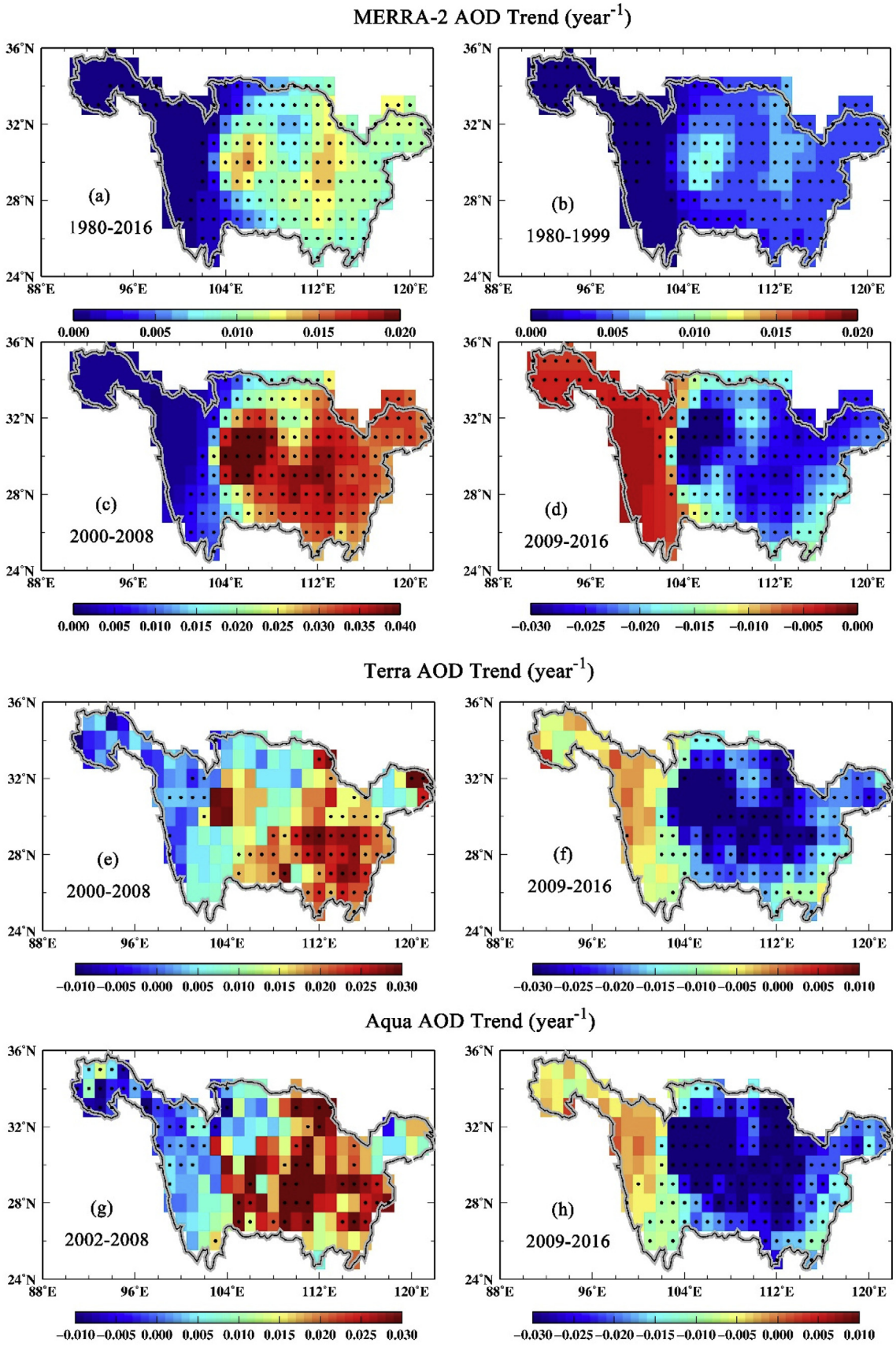

Fig. 7. Spatial patterns of AOD trends calculated from monthly mean observed MERRA-2, Terra and Aqua AOD values over YRB. The MERRA-2 AOD trends for 1980–2016 and for 1980-1999 are respectively depicted in Fig. 6 (a) and (b). The AOD trends for 2000-2008 from MERRA-2, Terra and Aqua are shown in Fig. 6 (c), (e) and (g), while their 2009-2016 AOD trends are presented in Fig. 6 (d), (f) and (h). Pixels with significant trend ($p < 0.05$) are marked with a black dot.

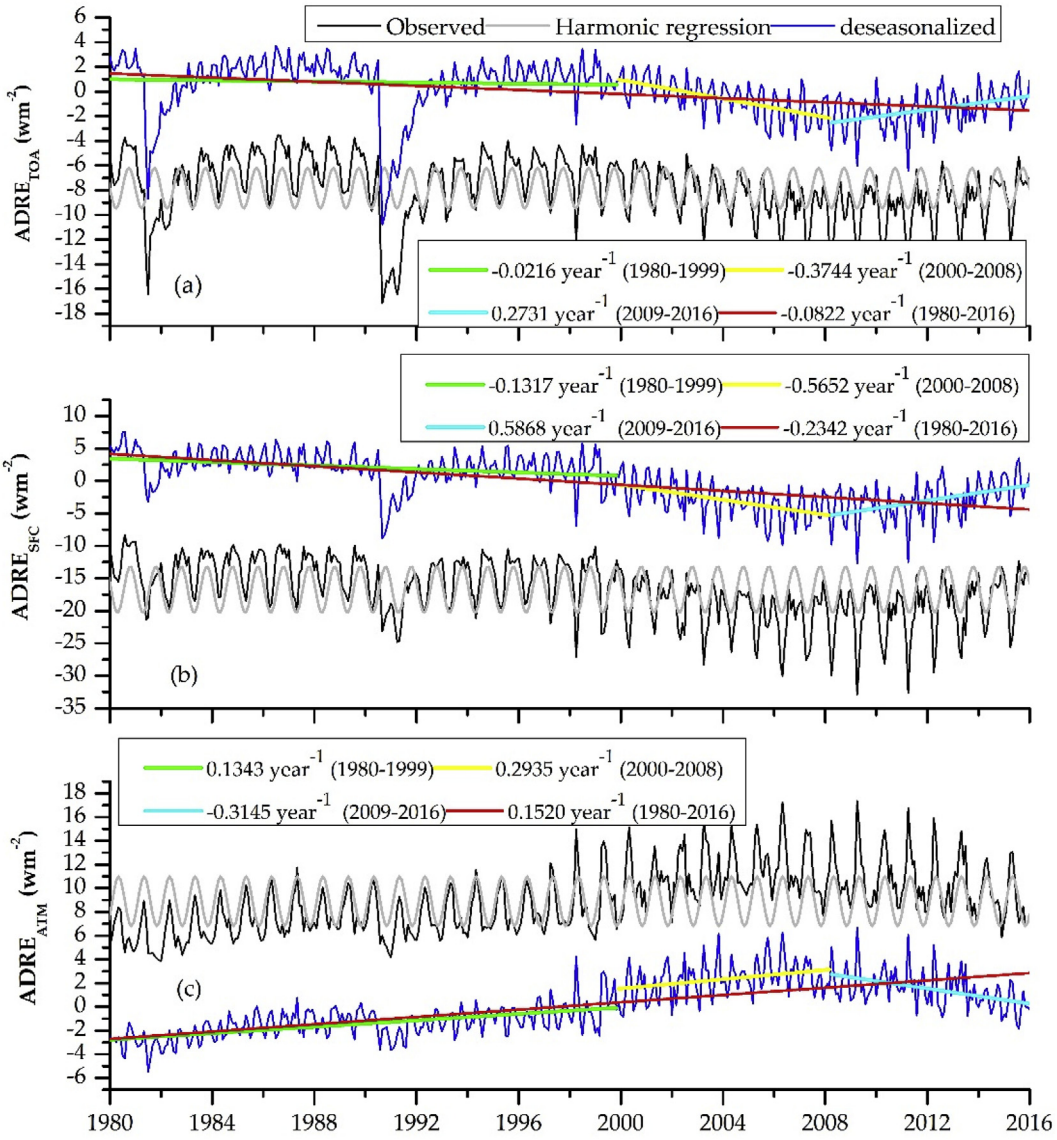

Fig. 8. Trend analysis of deseasonalized $ADRE_{TOA}$ (a), $ADRE_{SFC}$ (b) and $ADRE_{ATM}$ (c) derived from monthly mean MERRA-2 radiation reanalysis datasets from 1980 to 2016 over YRB. The deseasonalized ADRE values (blue) are calculated by subtracting the seasonal cycle (gray) from the observed ADRE (black). The ADRE seasonal cycle (gray) is quantified by the Harmonic regression. (For interpretation of the references to colour in this figure legend, the reader is referred to the Web version of this article.)

2016. In general, there is an increasing warming effect for aerosols at the ATM due to an upward $ADRE_{ATM}$ trend (0.1520 Wm^{-2} $year^{-1}$) for the entire study period.

The MERRA-2 ADRE spatial trends the TOA, SFC and ATM are further identified by a linear regression and depicted in Figs. 9–11, respectively. Overall, the spatial ADRE trends are consistent with their monthly variations (Fig. 8). The cooling (warming) effects at TOA and SFC (ATM) increase slightly for 1980-2016, increase strongly during 2000–2008 and decrease significantly during 2009–2016. However, during 2000–2008 (Figs. 9(c)-11(c)), the strongly increased cooling (warming) effects at the TOA and SFC (ATM) appear over the SS, CC and YRD. These regions are usually with high aerosol loadings (Fig. 3) and strong upward AOD trends (Fig. 7). Similarly, in Figs. 9(d)-11(d), the significantly decreased cooling (warming) effects at the TOA and SFC (ATM) from 2009 to 2016 also take place over the SS, CC and YRD, where there are high aerosol loadings and strong downward AOD trends. This confirms that even though ADRE may be impacted by the surface reflectance, water vapor and aerosol single scattering albedo reported by previous studies (Sundström et al., 2014; Biswas et al., 2017), changes in AOD from 1980 to 2016 over YRB are the main reason for the ADRE trend. Lately, Alfaro-Contreras et al. (2017) reported that regional shortwave ADRE trends at the TOA over global ocean were in good agreement with AOD trends by using the near-full MODIS (2000–2015), MISR (2000–2015), CALIOP (2006–2015) and CERES (2000–2015) data records.

3.3. Correlation analysis between AOD trend and its impact factors

3.3.1. Effect of NDVI on AOD trend

Fig. 12 (a) and (b) depict the annual mean NDVI spatial distribution and the spatial relationship between multi-year monthly NDVI and MERRA-2 AOD from 2000 to 2016 over YRB. The pixels ($1^\circ \times 1^\circ$) at 95% significant level detected by the T-test method are marked with a dot. Overall, there is a significant negative correlation ($R < -0.6$) between AOD and NDVI, especially over the CC and high mountains in the east of the SB. As observed by the previous researches, AOD is significantly impacted by NDVI, characterized by high aerosol loadings occur in the regions with sparse vegetation, such as the CC and YRD (Li

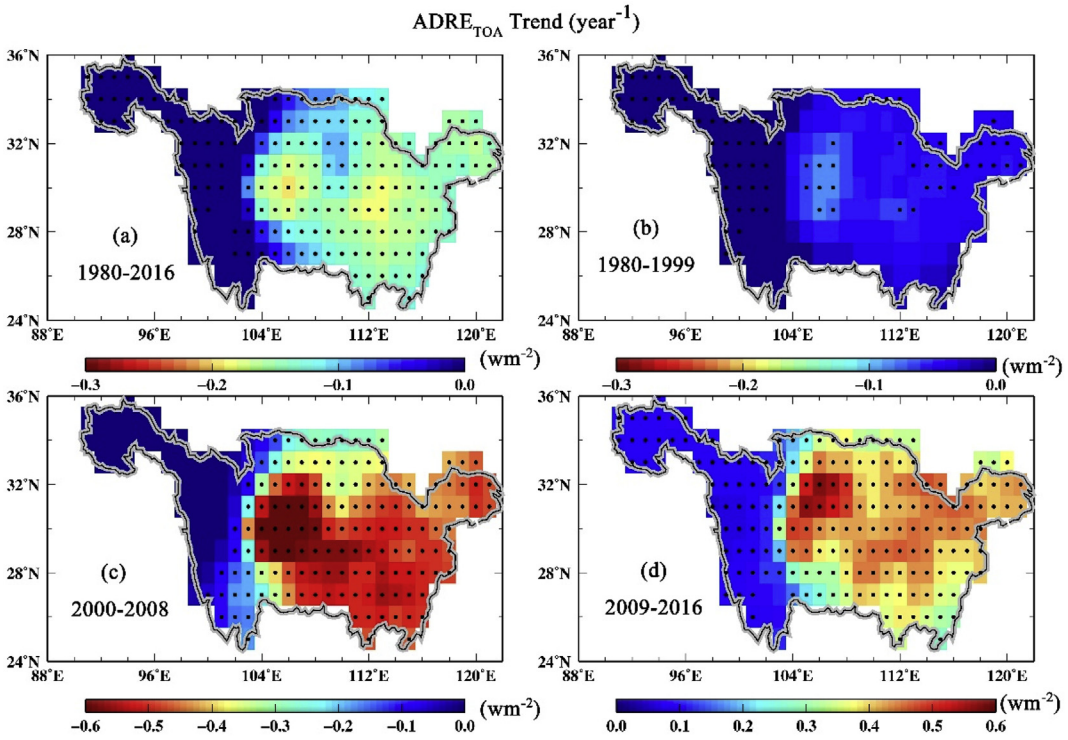

Fig. 9. Spatial patterns of ADRE$_{TOA}$ trends for the period of 1980–2016 (a), 1980–1999 (b), 2000–2008 (c) and 2009–2016 (d). They are calculated from monthly mean observed MERRA-2 radiation reanalysis datasets from 1980 to 2016 over YRB. Pixels (0.5° × 0.625°) with a significant trend ($p < 0.05$) detected by the MK method are marked with a black dot.

and Wang, 2014; He et al., 2016).

To further analyze whether changes in NDVI lead to the AOD trend over YRB, multi-year averaged NDVI trends are quantified to compare with AOD trends from 2000 to 2016. The corresponding results are shown in Fig. 12(c) and (d). The black lines in Fig. 12(c) represent insignificant NDVI trends detected by MK method, while the significant AOD trends in Fig. 12(d) are marked with a dot. As illustrated in Fig. 12 (c), there are significantly decreasing NDVI trends over the YRD and several areas in CC, probably due to the rapid urbanization. Piao et al. (2003) confirmed that rapid urbanization had reduced vegetation over

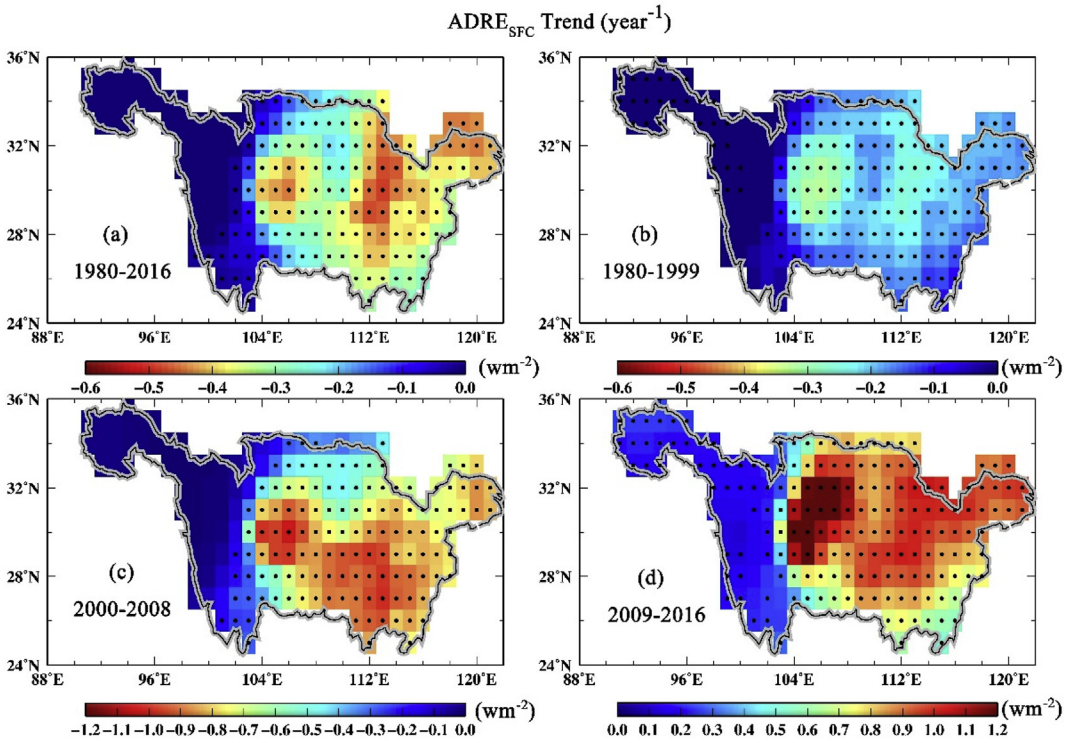

Fig. 10. Similar to Fig. 9, but for the ADRE$_{SFC}$ trend.

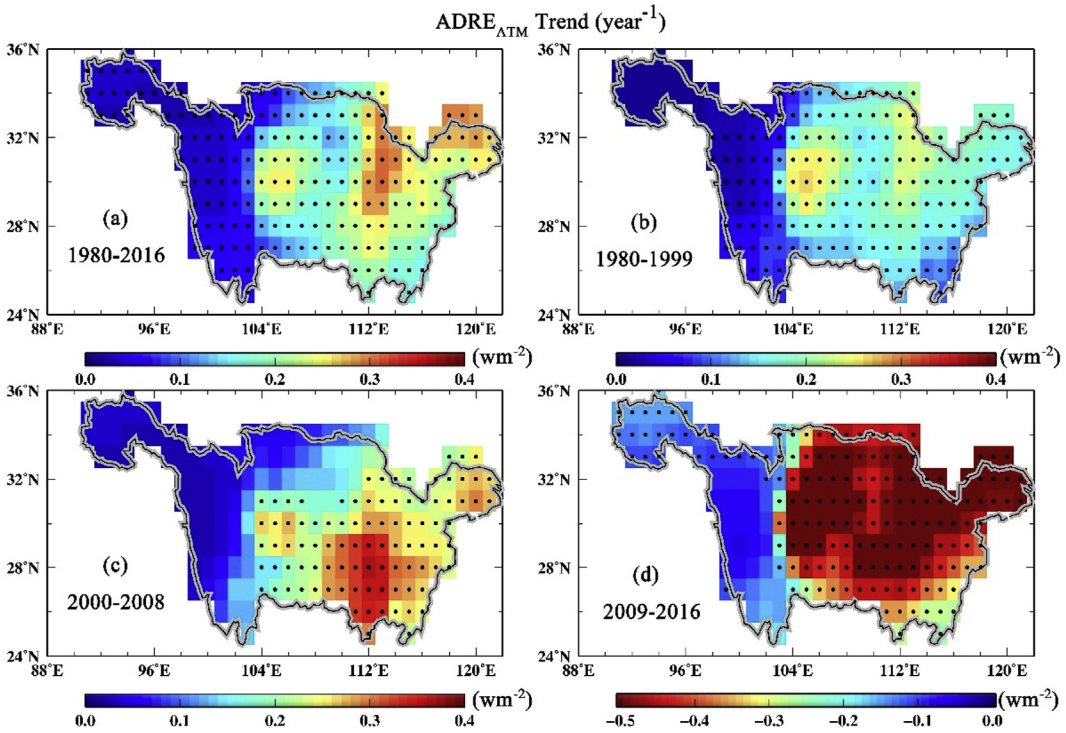

Fig. 11. Similar to Fig. 9, but for the ADRE$_{ATM}$ trend.

the YRD and Pearl River Delta, by using 18-year monthly NDVI data derived from the Global Inventory Monitoring and Modeling Studies (GIMMS). On the contrary, significantly increasing NDVI trends are observed over the mountains around the SB, where there are dense vegetation. The upward NDVI trends are probably response to a series of forest ecology projects over the middle and upper reaches of the Yangtze River launched by Chinese government since 1990s (Peng et al., 2014). Additionally, due to the negative correlation between NDVI and AOD, there should be significant upward AOD trends over those regions with decreasing NDVI trends, such as the YRD and a few areas of the CC, which has been confirmed by Fig. 12 (d). However, increasing NDVI in the mountains around the SB does not contribute to

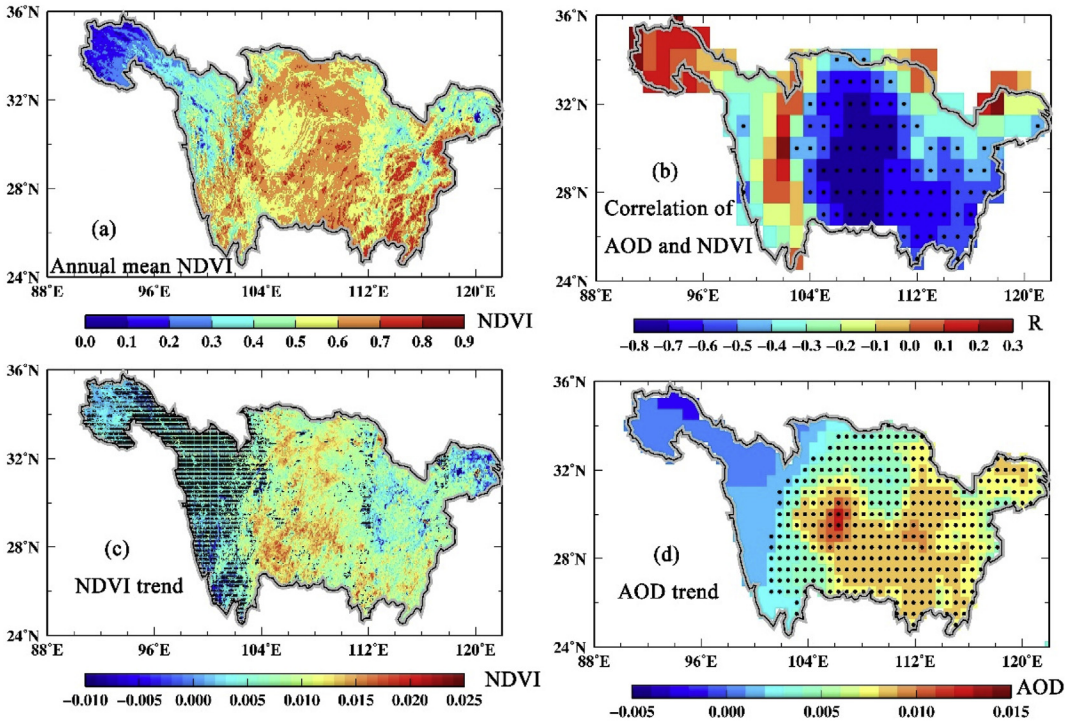

Fig. 12. Spatial patterns of (a) annual mean NDVI derived from MCD13 product with a spatial resolution of 0.05°, (b) correlation of the 17-year monthly NDVI and MERRA-2 AOD values, (c) annual NDVI trend and (d) annual AOD trend for the period of 2000–2016 over YRB. Notably, the significant correlation (b) and AOD trend (d) are marked with a black dot, while the black lines represent those insignificant NDVI trends (c).

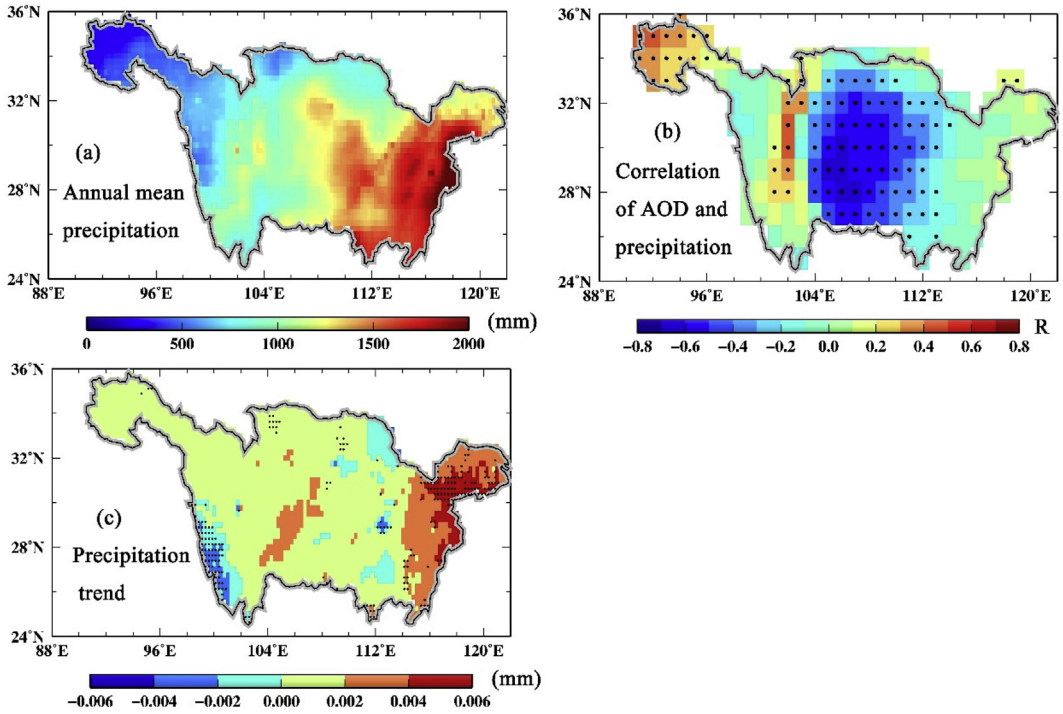

Fig. 13. Spatial patterns of (a) annual mean precipitation derived from TRMM 3B42 product with a spatial resolution of 0.25°, (b) correlation of the 17-year monthly precipitation and MERRA-2 AOD values, (c) annual precipitation trend for the period of 2000–2016 over YRB. Notably, the significant correlation (b) and precipitation trends (c) are marked with a black dot.

a decrease in AOD.

3.4. 2Effect of precipitation on AOD trend

As illustrated in Fig. 13(a), there is a distinct spatial distribution for precipitation, characterized by gradually deceasing from the southeast to the northwest of the YRB (Zhou et al., 2017). Despite of some exceptions shown in Fig. 13(b), the regional precipitation is negatively correlated with AOD ($R < -0.6$), especially over the SB. It is consistent with previous studies (Klingmüller et al., 2016; Boiyo et al., 2018). The reasons may be that precipitation can influence aerosols in the following ways: removing aerosol particles in the atmosphere, increasing soil moisture to inhibit dust emissions, and promoting plant growth to reduce aerosol loadings. Furthermore, as shown in Fig. 13(c), there are no significant trends in precipitation, neither positive nor negative, except several pixels over the YRD and the SYR. Obviously, comparing with AOD trends (Fig. 12(d)), the precipitation trends don't exhibit an opposite spatial pattern. In other words, even though AOD is significantly influenced by the regional precipitation, changes in precipitation alone are unlikely to contribute to increases in AOD over the YRB from 2000 to 2016.

3.4.1. Effect of GDP and PD on AOD trend

Fig. 14(a) exhibits the annual mean GDP spatial pattern of YRB from 2000 to 2015. High GDP appears over the regions with rapid economic development, such as the YRD, CC and SB. Comparing with Fig. 3(a), it is consistent with multi-year averaged AOD spatial distribution, which is further confirmed by Fig. 14(b). As illustrated in Fig. 14(b), there are significant positive correlations ($R > 0.8$) between multi-year averaged GDP and MERRA-2 AOD over most areas of YRB. Furthermore, to identify whether changes in GDP contribute to the AOD trend, the annual GDP trend is also quantified by a linear regression and the corresponding result is shown in Fig. 14(c). The pixels marked with gray lines represent those insignificant GDP trend based on the MK method. It is evident that GDP exhibits similar spatial trends with the MERRA-2 AOD shown in Fig. 12(d). To a certain extent, significantly increasing GDP leads to the upward AOD trend over the YRD, CC and SB for 2000–2015.

Similar to GDP, Fig. 15(b) also shows a significant positive relationship ($R > 0.8$) between multi-year averaged PD and MERRA-2 AOD over the SB and CC. Furthermore, the PD (Fig. 15(c)) exhibits a significantly increasing trend over the YRD, which leads to the growth of AOD over this region. However, fragmented PD patterns are observed over the SB and CC, where increasing and decreasing trends in PD are intertwined. The reasons are as follows. On one hand, the PD spatial trend is attributed to the internal migration of the YRB, characterized by the inflow of rural labor force into the provincial capital city and metropolitan areas (such as the YRD) (Li et al., 2014b; Shen et al., 2018). On the other hand, it may be due to the use of the spatial population datasets of 1 km × 1 km. Although it is conducive to solving the disconnection between population data and its spatial regions, the relative error of the spatial population data is about 4.5%–13.6% compared with the census data (Fu et al., 2014). In summary, even though the AOD is strongly positively related with the PD, changes in PD alone is unlikely to be the main reason for AOD increasing trends over the SB and CC from 2000 to 2015.

4. Conclusion

Using the monthly MODIS and MERRA-2 aerosol reanalysis datasets, we perform the trend analysis of AOD and ADRE both temporally and spatially, and further explore the potential factors leading to changes in AOD over the YRB since 1980. First of all, in order to estimate the accuracy of the MERRA-2 aerosol reanalysis data, the comparison between MERRA-2 AOD and ground-based AOD derived from four CARSNET sites over the YRB is implemented for the period 2007–2012. High correlation coefficient ($R = 0.9$) provides confidence in using MERRA-2 datasets.

Regional analyses corroborate that high aerosol loadings ($AOD > 0.5$) are observed over the YRD, CC and SB, where there are frequently anthropogenic activities. Similarly, over these regions, there are also strong cooling (warming) effects at the TOA and SFC (ATM),

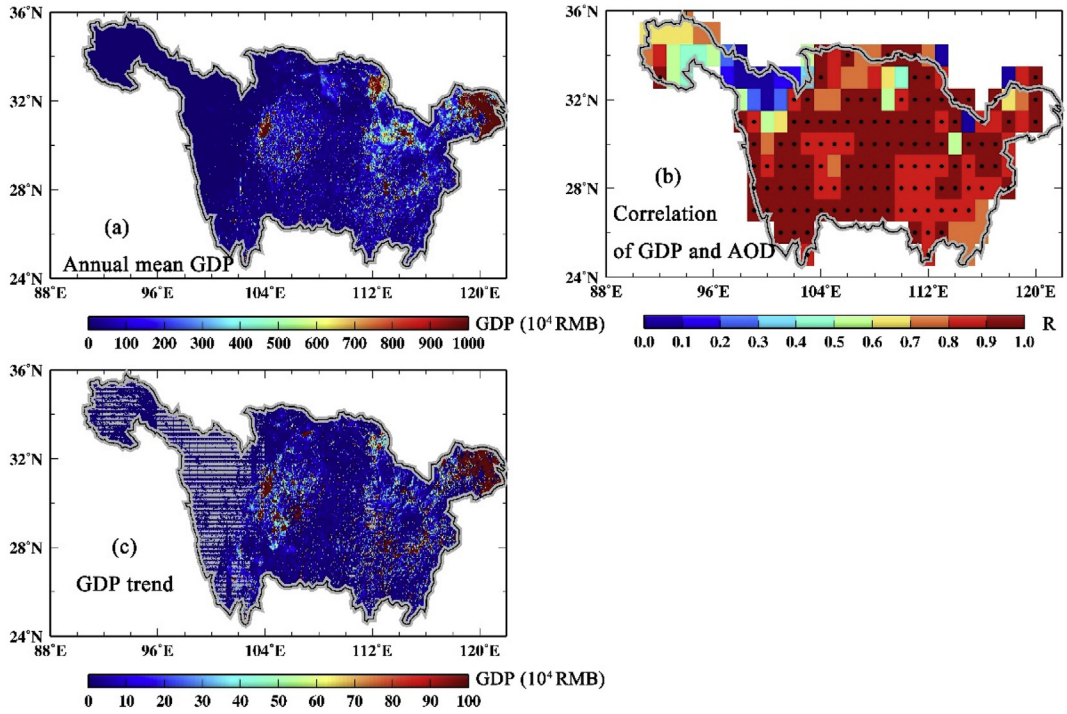

Fig. 14. Spatial patterns of (a) annual mean GDP with a spatial resolution of 1 km, (b) correlation of the multi-year averaged GDP and MERRA-2 AOD values, (c) annual GDP trend for the period of 2000–2015 over YRB. Notably, the significant correlation (b) is marked with a black dot, while the gray lines (c) represent those insignificant GDP trend.

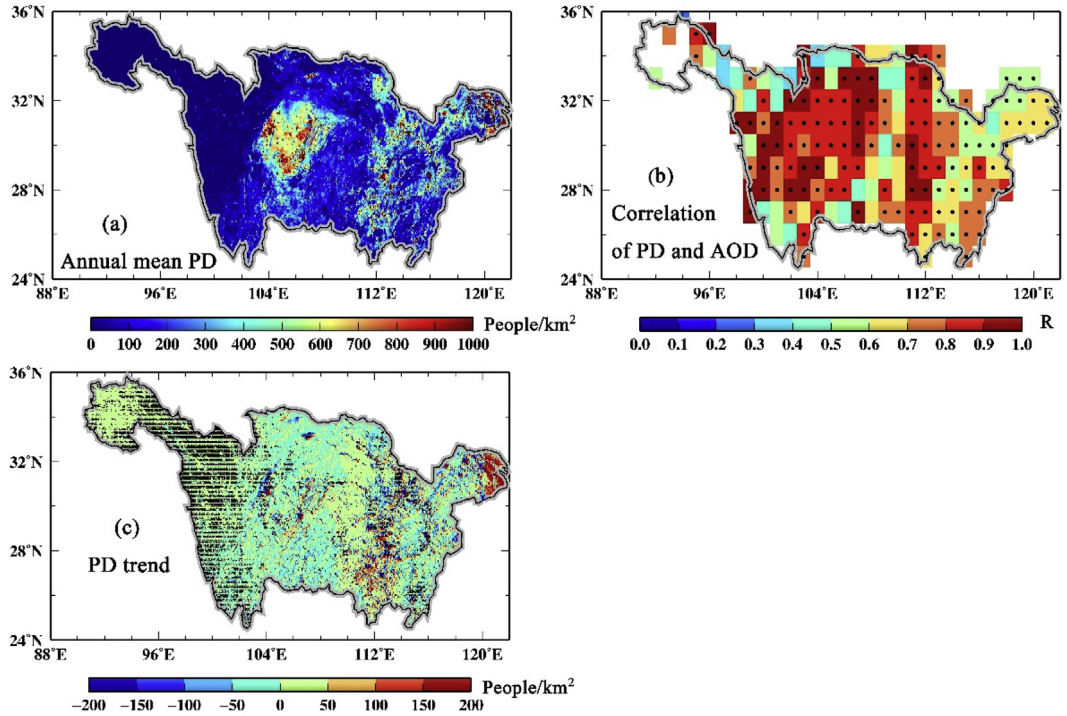

Fig. 15. Similar to Fig. 14, but for the population density (PD).

along with their corresponding annual mean $ADRE_{TOA} < -10\ wm^{-2}$, $ADRE_{SFC} < -20\ wm^{-2}$, and $ADRE_{ATM} > 12\ wm^{-2}$ in clear sky. Therefore, ADRE on the whole earth-atmosphere system is strongly associated with AOD. It is characterized by significant negative correlation ($R < -0.8$, $p < 0.05$) of AOD with $ADRE_{TOA}$ and $ADRE_{SFC}$ in most areas of the YRB. However, the significant positive relationship ($R > 0.8$, $p < 0.05$) between AOD and $ADRE_{TOA}$ is observed over the middle and lower reaches of the YRB, and gradually decreases from the southeast to the northwest.

There are similar AOD trends retrieved from MERRA-2, Terra and Aqua: strong upward trend during 2000–2008 (0.0201, 0.0138 and 0.0131 $year^{-1}$) and significant downward trend during 2009–2016 (−0.0185, −0.0200 and −0.0214 $year^{-1}$). Nevertheless, a slight upward trend in AOD is observed for the entire study period (0.0065

year^{-1}). The transition in AOD trend from increase to decrease during 2008–2009 is probably related with the 2008 Olympic Games, when a series of emission reduction measures have been implemented. For example, SO_2, NO_x and soot (dust) emissions from major cities of the YRB begin to decrease continuously since 2006. In terms of the spatial AOD trend, it is consistent with its temporal variation. In particularly, the strong upward (downward) AOD trends during 2000–2008 (2009–2016) are observed over the YRD, CC and SB. However, there is an upward AOD trend over the SYB during 2009–2016 observed by Terra and Aqua, an alarm for air pollution in this region.

In terms of the ADRE trend, it is consistent with AOD trend both temporally and spatially. The cooling (warming) effects at the TOA and SFC (ATM) are observed to increase strongly by −0.3744 and −0.5652 (0.2935) wm^{-2} year^{-1}during 2000–2008, and decrease significantly by 0.2731 and 0.5868 (−0.3145) wm^{-2} year^{-1} during 2009–2016. This confirms that changes in AOD seem to be the dominant factor for ADRE trends over the YRB from 1980 to 2016.

Correlation analyses identify that there are significant negative (positive) relationship of NDVI and precipitation (GDP and PD) with AOD over most areas of the YRB for the period of 2000–2016. However, no significant trends in precipitation are detected, suggesting that changes in precipitation alone are unlikely to lead to an increase in AOD. Similarly, although regional AOD is deeply influenced by PD, fragmented patterns of PD trends over the SB and CC are unlikely to be the major reason for the upward trend in AOD. Nevertheless, NDVI trends caused by rapid urbanization over the YRD and CC are significantly reduced, resulting in an increase in AOD over these regions. Besides, GDP spatial trends are strongly consistent with changes in AOD over the whole YRB. It confirms that the increase in AOD from 2000 to 2015 is to some extent caused by GDP growth, especially over the YRD, CC and SB.

Acknowledgments

This work was financially supported by National Natural Science Foundation of China (No.41601044, No.41571400), the Special Fund for Basic Scientific Research of Central Colleges, China University of Guelph, Wuhan (No.CUG150631, CUGL170401, CUGCJ1704), and the Opening Foundation of Key Laboratory of Middle Atmosphere and Global Environment Observation (LAGEO), Institute of Atmospheric Physics, Chinese Academy of Sciences. We would like to thank the NASA Global Modeling and Assimilation Office for providing the MERRA-2 aerosol reanalysis data. Concerning to natural and socio-economic factor datasets used in this paper, we are particularly grateful to Data Center for the Resources and Environmental Sciences, Chinese Academy of Sciences.

References

Alfaro-Contreras, R., Zhang, J., Reid, J.S., Sundar, C., 2017. A study of 15–year aerosol optical thickness and direct shortwave aerosol radiative effect trends using MODIS, MISR, CALIOP and CERES. Atmos. Chem. Phys. 17, 13849. https://doi.org/10.5194/acp-17-13849-2017.

Bilal, M., Nichol, J.E., 2015. Evaluation of MODIS aerosol retrieval algorithms over the Beijing–Tianjin–Hebei region during low to very high pollution events. J. Geophys. Res. Atmos. 120, 7941–7957.

Bilal, M., Nazeer, M., Nichol, J.E., 2017a. Validation of MODIS and VIIRS derived aerosol optical depth over complex coastal waters. Atmos. Res. 186, 43–50.

Bilal, M., Nichol, J.E., Wang, L., 2017b. New customized methods for improvement of the MODIS C6 Dark Target and Deep Blue merged aerosol product. Remote Sens. Environ. 197, 115–124.

Bilal, M., Nazeer, M., Qiu, Z., Ding, X., Wei, J., 2018. Global validation of MODIS C6 and C6. 1 merged aerosol products over diverse vegetated surfaces. Rem. Sens. 10, 475. https://doi.org/10.3390/rs10030475.

Biswas, J., Pathak, B., Patadia, F., Bhuyan, P.K., Gogoi, M.M., Babu, S.S., 2017. Satellite–retrieved direct radiative forcing of aerosols over North–East India and adjoining areas: climatology and impact assessment. Int. J. Climatol. 37, 298–317.

Boiyo, R., Kumar, K.R., Zhao, T., 2018. Spatial variations and trends in AOD climatology over East Africa during 2002–2016: a comparative study using three satellite data sets. Int. J. Climatol. https://doi.org/10.1002/joc.5446.

Buchard, V., da Silva, A.M., Colarco, P.R., Darmenov, A., Randles, C.A., Govindaraju, R., Torres, O., Campbell, J., Spurr, R., 2015. Using the OMI aerosol index and absorption aerosol optical depth to evaluate the NASA MERRA Aerosol Reanalysis. Atmos. Chem. Phys. 15, 5743–5760.

Buchard, V., da Silva, A.M., Randles, C.A., Colarco, P., Ferrare, R., Hair, J., Hostetler, C., Tackett, J., Winker, D., 2016. Evaluation of the surface PM2.5 in version 1 of the nasa MERRA aerosol reanalysis over the United States. Atmos. Environ. 125, 100–121.

Buchard, V., Randles, C.A., da Silva, A.M., Darmenov, A., Colarco, P.R., Govindaraju, R., Ferrare, R., Hair, J., Beyersdorf, A.J., Ziemba, L.D., Yu, H., 2017. The MERRA–2 aerosol reanalysis, 1980 onward. Part II: evaluation and case studies. J. Clim. 30, 6851–6872.

Charlson, R.J., Langner, J., Rodhe, H., Leovy, C.B., Warren, S.G., 1991. Perturbation of the Northern–Hemisphere radiative balance by backscattering from anthropogenic sulfate aerosols. Tellus A 43, 152–163.

Che, H., Zhang, X., Chen, H., Damiri, B., Goloub, P., Li, Z., Li, D., 2009. Instrument calibration and aerosol optical depth validation of the China Aerosol Remote Sensing Network. J. Geophys. Res. Atmos. 114, D3. https://doi.org/10.1029/2008JD011030.

Che, H., Xia, X., Zhu, J., Li, Z., Dubovik, O., Holben, B., Blarel, L., 2014. Column aerosol optical properties and aerosol radiative forcing during a serious haze-fog month over North China Plain in 2013 based on ground-based sunphotometer measurements. Atmos. Chem. Phys. 14, 2125–2138.

Che, H., Zhang, X.Y., Xia, X., Goloub, P., Holben, B., Zhao, H., Wang, Y., Zhang, X.C., Wang, H., Blarel, L., Damiri, B., 2015. Ground–based aerosol climatology of China: aerosol optical depths from the China aerosol remote sensing network (CARSNET) 2002–2013. Atmos. Chem. Phys. 15, 7619–7652.

Christopher, S.A., 2011. Satellite remote sensing methods for estimating clear Sky shortwave Top of atmosphere fluxes used for aerosol studies over the global oceans. Remote Sens. Environ. 125, 3002–3006.

De Leeuw, G., Sogacheva, L., Rodriguez, E., Kourtidis, K., Georgoulias, A.K., Alexandri, G., Amiridis, V., Proestakis, E., Marinou, E., Xue, Y., 2017. Two decades of satellite observations of AOD over mainland China. Atmos. Chem. Phys. Discuss. 2017, 1–33.

Dutton, E.G., Christy, J.R., 1992. Solar radiative forcing at selected locations and evidence for global lower tropospheric cooling following the eruptions of El Chichón and Pinatubo. Geophys. Res. Lett. 19, 2313–2316.

Feng, N., Christopher, S.A., 2014. Clear sky direct radiative effects of aerosols over Southeast Asia based on satellite observations and radiative transfer calculations. Remote Sens. Environ. 152, 333–344.

Fu, J.Y., Jiang, D., Huang, Y.H., 2014. 1 km grid population dataset of China (2005, 2010). Glob. Chang. Res. Data Publ. Repos. 69, 136–139 (in Chinese).

Guo, J., Xia, F., Zhang, Y., Liu, H., Li, J., Lou, M., He, J., Yan, Y., Wang, F., Min, M., Zhai, P., 2017. Impact of diurnal variability and meteorological factors on the PM 2.5–AOD relationship: implications for PM 2.5 remote sensing. Environ. Pollut. 221, 94–104.

He, Q., Zhang, M., Huang, B., 2016. Spatio–temporal variation and impact factors analysis of satellite–based aerosol optical depth over China from 2002 to 2015. Atmos. Environ. 129, 79–90.

He, L., Wang, L., Lin, A., Zhang, M., Bilal, M., Tao, M., 2017. Aerosol optical properties and associated direct radiative forcing over the Yangtze River basin during 2001–2015. Rem. Sens. 9, 746. https://doi.10.3390/rs9070746.

He, L., Wang, L., Lin, A., Zhang, M., Bilal, M., Wei, J., 2018. Performance of the NPP–VIIRS and aqua–MODIS aerosol optical depth products over the Yangtze River basin. Rem. Sens. 10, 117. https://doi.10.3390/rs10010127.

Huang, Y., Chameides, W.L., Dickinson, R.E., 2007. Direct and indirect effects of anthropogenic aerosols on regional precipitation over East Asia. J. Geophys. Res. 122, D03212. https://doi.org/10.1029/2006JD007124.

Kang, N., Kumar, K.R., Yu, X., Yin, Y., 2016. Column–integrated aerosol optical properties and direct radiative forcing over the urban–industrial megacity Nanjing in the Yangtze River Delta, China. Environ. Sci. Pollut. Res. 23, 17535–17552.

Klingmüller, K., Pozzer, A., Metzger, S., Stenchikov, G.L., Lelieveld, J., 2016. Aerosol optical depth trend over the Middle East. Atmos. Chem. Phys. 16, 5063–5073.

Li, J., Carlson, B.E., Dubovik, O., Lacis, A.A., 2014a. Recent trends in aerosol optical properties derived from AERONET measurements. Atmos. Chem. Phys. 14, 12271–12289.

Li, L., Wang, Y., 2014. What drives the aerosol distribution in Guangdong–the most developed province in Southern China? Sci. Rep. 4, 5972. https://doi.10.1038/srep05972.

Li, Y., Liu, H., Tang, Q., Lu, D., Xiao, N., 2014b. Spatial–temporal patterns of China's interprovincial migration, 1985–2010. J. Geogr. Sci. 24, 907–923.

Mehta, M., Singh, R., Singh, A., Singh, N., 2016. Recent global aerosol optical depth variations and trends—a comparative study using MODIS and MISR level 3 datasets. Remote Sens. Environ. 181, 137–150.

McCormick, M.P., Swissler, T.J., 1983. Stratospheric aerosol mass and latitudinal distribution of the El Chichon eruption cloud for October 1982. Geophys. Res. Lett. 10, 877–880.

Patadia, F., Gupta, P., Christopher, S.A., 2008. First observational estimates of global clear sky shortwave aerosol direct radiative effect over land. Geophys. Res. Lett. 35, 228–236.

Peng, S.S., Piao, S., Zeng, Z., Ciais, P., Zhou, L., Li, L.Z., Myneni, R.B., Yin, Y., Zeng, H., 2014. Afforestation in China cools local land surface temperature. P. Natl. Acad. Sci. 121, 2915–2919.

Piao, S., Fang, J., Zhou, L., Guo, Q., Henderson, M., Ji, W., Li, Y., Tao, S., 2003. Interannual variations of monthly and seasonal normalized difference vegetation index (NDVI) in China from 1982 to 1999. J. Geophys. Res. Atmos. 108, D14. https://doi.org/10.1029/2002JD002848.

Randles, C.A., da Silva, A.M., Buchard, V., Colarco, P.R., Darmenov, A., Govindaraju, R., Smirnov, A., Holben, B., Ferrare, R., Hair, J., Shinozuka, Y., 2017. The MERRA–2 aerosol reanalysis, 1980 onward. Part I: system description and data assimilation evaluation. J. Clim. 30, 6823–6850.

Sayer, A.M., Munchak, L.A., Hsu, N.C., Levy, R.C., Bettenhausen, C., Jeong, M.J., 2014. MODIS Collection 6 aerosol products: comparison between Aqua's e-Deep Blue, Dark Target, and "merged" data sets, and usage recommendations. J. Geophys. Res. Atmos. 119, 13–965.

Shen, H., Chen, Y., Russell, A.G., Hu, Y., Shen, G., Yu, H., Henneman, L.R., Ru, M., Huang, Y., Zhong, Q., Chen, Y., 2018. Impacts of rural worker migration on ambient air quality and health in China: from the perspective of upgrading residential energy consumption. Environ. Int. 113, 290–299.

Sundström, A.M., Arola, A., Kolmonen, P., Xue, Y., de Leeuw, G., Kulmala, M., 2014. On the use of satellite remote sensing based approach for determining aerosol direct radiative effect over land: a case study over China. Atmos. Chem. Phys. 15, 505–518.

Tao, M., Chen, L., Li, R., Wang, L., Wang, J., Wang, Z., Tang, G., Tao, J., 2016. Spatial oscillation of the particle pollution in eastern China during winter: implications for regional air quality and climate. Atmos. Environ. 144, 100–120.

Tao, R., Che, H.Z., Chen, Q.L., Tao, J., Wang, Y.Q., Sun, J.Y., Wang, H., Zhang, X.Y., 2014. Study of aerosol optical properties based on ground measurements over Sichuan Basin, China. Aerosol Air Qual. Res. 14, 905–915.

Wang, L., Gong, W., Xia, X., Zhu, J., Li, J., Zhu, Z., 2015. Long–term observations of aerosol optical properties at Wuhan, an urban site in Central China. Atmos. Environ. 101, 94–102.

Wei, J., Sun, L., Huang, B., Bilal, M., Zhang, Z., Wang, L., 2017. Verification, improvement and application of aerosol optical depths in China Part 1: inter–comparison of NPP–VIIRS and Aqua–MODIS. Atmos. Environ. 175, 221–233.

Xia, X., Che, H., Zhu, J., Chen, H., Cong, Z., Deng, X., Fan, X., Fu, Y., Goloub, P., Jiang, H., Liu, Q., 2016. Ground–based remote sensing of aerosol climatology in China: aerosol optical properties, direct radiative effect and its parameterization. Atmos. Environ. 124, 243–251.

Yu, X., Lü, R., Kumar, K.R., Ma, J., Zhang, Q., Jiang, Y., Kang, N., Yang, S., Wang, J., Li, M., 2016. Dust aerosol properties and radiative forcing observed in spring during 2001–2014 over urban Beijing, China. Environ. Sci. Pollut. Res. 23, 15432–15442.

Young, P.C., Pedregal, D.J., Tych, W., 1999. Dynamic harmonic regression. J. Forecast. 18, 369–394.

Zhang, J., Reid, J.S., 2010. A decadal regional and global trend analysis of the aerosol optical depth using a data–assimilation grade over–water MODIS and Level 2 MISR aerosol products. Atmos. Chem. Phys. 10, 10949–10963.

Zhang, J., Reid, J.S., Alfaro-Contreras, R., Xian, P., 2017a. Has China been exporting less particulate air pollution over the past decade? Geophys. Res. Lett. 44, 2941–2948.

Zhang, M., Ma, Y., Gong, W., Wang, L., Xia, X., Che, H., Hu, B., Liu, B., 2017b. Aerosol radiative effect in UV, VIS, NIR, and SW spectra under haze and high–humidity urban conditions. Atmos. Environ. 166, 9–21.

Zhang, M., Ma, Y., Wang, L., Gong, W., Hu, B., Shi, Y., 2018. Spatial-temporal characteristics of aerosol loading over the Yangtze River Basin during 2001–2015. Int. J. Climatol. 38, 2138–2152.

Zhou, H., Luo, Z., Tangdamrongsub, N., Wang, L., He, L., Xu, C., Li, Q., 2017. Characterizing drought and flood events over the Yangtze River basin using the HUST–grace2016 solution and ancillary data. Rem. Sens. 9, 1100. https://doi:10.3390/rs9121200.

Zhuang, B.L., Wang, T.J., Li, S., Liu, J., Talbot, R., Mao, H.T., Yang, X.Q., Fu, C.B., Yin, C.Q., Zhu, J.L., Che, H.Z., 2014. Optical properties and radiative forcing of urban aerosols in Nanjing, China. Atmos. Environ. 83, 43–52.